

LARGE DYNAMIC RANGE NANOPositionING USING ITERATIVE LEARNING CONTROL

G. PARMAR¹, D.B. HIEMSTRA, AND S. AWTAR
Precision Systems Design Laboratory
Mechanical Engineering, University of Michigan
Ann Arbor, MI 48109

ABSTRACT

This paper presents the control system design and tracking performance of a large range single-axis nanopositioning system that is based on a moving magnet actuator and flexure bearing. While the physical system is designed to be free of friction and backlash, the nonlinearities in the electromagnetic actuator as well as the harmonic distortion in the drive amplifier restrict the achievable tracking performance for dynamic command following. It is shown that linear feedback proves to be inadequate due to limitations arising from the low open-loop bandwidth of the physical system. For periodic commands, like those used in scanning applications, the component of the tracking error due to the nonlinearities is deterministic and repeats every period. Therefore, an iterative learning controller (ILC) is designed and implemented in conjunction with linear feedback to reduce this periodic tracking error by more than three orders of magnitude. Experimental results demonstrate the effectiveness of this ILC in achieving 18nm RMS tracking error over 6mm range in response to a 2Hz band-limited triangular command. This corresponds to a dynamic range of 10^5 .

INTRODUCTION

Nanopositioning is one of the key enabling technologies for measurement and manipulation of matter at the molecular scale [1]. Because of their nanometric ($< 10\text{nm}$) motion quality (accuracy, precision, and resolution), nanopositioning systems are employed in various sensitive applications that require relative scanning motion between a probe and a substrate. However, one of the main drawbacks of currently available nanopositioning systems is their small motion range of a few hundred microns per axis [2, 3]. Increasing this range to several millimeters will enable large-size substrates in several applications such as scanning probe microscopy [4], scanning probe lithography [5], and nanometrology [6].

The ongoing research efforts in the area of large range translational nanopositioning systems can be broadly classified into three categories. The first category is of positioning systems that have friction and backlash in one or more of their physical components, such as the bearing or transmission. The motion stage in these cases is supported by rolling [7-9] or sliding [10-12] guideways. Either direct-drive linear motors [8, 11, 12] or rotary motors coupled with lead-screw drives [7, 9, 10, 13] are used for actuation. For these systems, linear feedback controllers do not offer adequate positioning performance due to the nonlinear and parameter-varying characteristics of friction, especially in the micro-dynamic regime [14]. Implementation of advanced controllers [7, 9, 12] has shown some performance improvements over linear feedback.

To overcome the performance limitations associated with friction, another approach has been to mount a small range, high motion quality positioning system (fine stage) on top of a large range, friction-based traditional motion system (coarse stage) [8, 10, 11, 13]. The idea is to use the fine stage to compensate for the positioning errors of the coarse stage, thereby improving the overall positioning performance. The major challenge here lies in the control system design to ensure coordination between the coarse and fine motion systems [13].

Separately, there has been a considerable effort focused on positioning systems that are based on non-contact and frictionless operation. These systems rely on magnetic [15-17], aerostatic [18-20], or flexure bearings [2, 21, 22] for motion guidance, and generally employ direct-drive electromagnetic actuators. Each of these presents unique control design challenges to achieve nanometric motion quality. For example, electromagnetic bearings and well as actuators suffer from force-stroke nonlinearities [16]. Also, the noise and distortion in the actuator driver degrades the positioning performance [22]. Air bearings exhibit sustained vibrations in both load-bearing as well as motion direction [23,

¹ Corresponding Author (parmar@umich.edu, 734-239-2928)

24]. In flexure bearings, poorly damped high frequency poles and zeros limits the closed-loop performance [2]. Additionally, they require higher actuation effort to overcome the spring stiffness.

The motion quality of nanopositioning systems is dictated by the tracking error, which is the difference between the commanded and the measured position. Tracking error may be evaluated for either point-to-point positioning commands or for path-following commands. Point-to-point positioning is concerned with moving the motion stage from one point to another and staying there for some finite period of time. Only the final position is relevant and the path taken to reach that position is not. On the other hand, in the more general case of path-following such as raster scanning, the motion stage is moved along a pre-defined trajectory in time and space, and position at each point along this trajectory is important. Obtaining nanometric tracking performance for such dynamic commands is relatively challenging because a linear controller may not provide adequate command following and disturbance rejection over a desired finite frequency range. While many of the above-mentioned references [2, 7-9, 15-17, 19-22] have reported large range (> 1mm) and high resolution (< 10nm *Root Mean Square* or RMS) for point-to-point positioning commands, only a few have shown nanometric positioning performance for dynamic commands over a large motion range (Table 1). It should be noted that due to differences in the range, frequency content, and type of command trajectory used, it is not possible to compare the tracking performances of these systems in a consistent manner.

In recent work [25], the design, fabrication, and testing of a single-axis nanopositioning system employing a flexure bearing and moving magnet actuator was presented. Point-to-point

positioning performance was shown with a lead-lag controller to be within 4nm (RMS) over the motion range of 10mm. However, nonlinearities associated with the actuator as well as the driver resulted in inadequate tracking performance in response to dynamic commands. In this paper, advanced controls design and implementation is presented to overcome these nonlinearities in order to achieve nanometric tracking performance for dynamic commands over a large motion range. First, the physical system is described along with its open-loop characterization. Next, it is shown that a linear feedback controller by itself offers inadequate performance. This is because of the limited sensitivity reduction that is possible by employing a feedback loop, given actuator saturation and low open-loop bandwidth of the system. For scanning-type applications, in which the command is a periodic signal, the deterministic part of the error, arising due to nonlinearities, also repeats every period. This provides the motivation to employ iterative learning control (ILC) to reduce the repeating portion of the tracking error. Since its inception in early eighties, ILC has seen tremendous applications in the fields of robotics [26] and motion systems [27, 28]. Some of the advantages of ILC include its linear formulation, minimal knowledge of plant dynamics, simple design and implementation, and that fact that it can be applied to any existing feedback control system [26]. A brief introduction to ILC is presented followed by the design and implementation of a P-type iterative learning controller in conjunction with the existing feedback controller. Experimental results are reported that demonstrate more than three orders of magnitude reduction in the tracking error while following dynamic commands, when compared to the performance obtained with a linear feedback controller only.

TABLE 1. DYNAMIC TRACKING PERFORMANCE IN LARGE RANGE NANOPOSITIONING SYSTEMS

Reference	Motion Range (mm)	Bearing	Actuator / Transmission	Reference Command	Tracking Error (nm)
Buice et al. [10]	50	Linear guide (coarse), flexure (fine)	DC motor with leadscrew (coarse), PZT (fine)	2.5mm sine @ 0.01Hz	45
Choi et al. [11]	–	Linear guide (coarse), air bearing (fine)	Linear motor (coarse), voice coil (fine)	20mm/s constant velocity, 300mm motion range	±150
Michellod et al. [13]	70	Flexure (coarse and fine)	Stepper motor with leadscrew (coarse), PZT (fine)	10µm, 200Hz Kolmogorov signal	8 (RMS)
Maeda et al. [20]	10	Air bearing	Voice coil	±3mm band-limited triangular profile @ 5Hz	±5
Zschaeck et al. [12]	200	Linear guide	Linear motor	1mm/s constant velocity, 10mm motion range	15 (RMS)
Fukada et al. [22]	1	Flexure	Moving magnet actuator	0.125mm/s constant velocity, 0.5mm motion range	±50
Kim et al. [16]	5	Electromagnetic	Electromagnetic	2.5mm/s constant velocity, 5mm motion range	25
This Paper	10	Flexure	Moving magnet actuator	±3mm band-limited triangular profile @ 2Hz	18 (RMS)

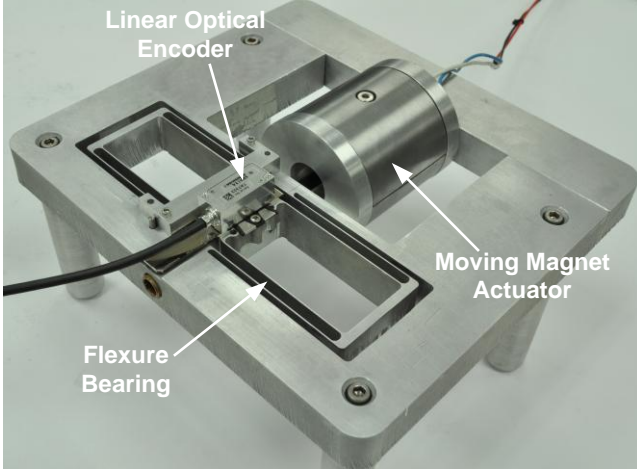


FIGURE 1. SINGLE-AXIS NANOPositioning SYSTEM

PHYSICAL SYSTEM

The single-axis nanopositioning system used in this work is shown in Figure 1. This setup consists of a symmetric double parallelogram flexure bearing and a moving magnet actuator (MMA). A linear optical encoder (RELM scale, Si-HN-4000 Read-head, and SIGNUM Interface from Renishaw) with 4nm (RMS) resolution is used for position measurement and feedback. The physical construction of the system provides frictionless and backlash-free motion over a motion range of 10mm. The detailed design and fabrication of the experimental setup can be found in previous work [25]. A custom-made voltage amplifier (based on the MP111 power-OpAmp from Cirrus Logic) with a gain of 5V/V and a bandwidth of over 10kHz is used to drive the MMA. The control system is implemented on a real-time hardware (DS1103 from DSpace) equipped with 16-bit DAC. The sampling frequency and the loop rate are fixed at 10kHz.

The open-loop frequency response of this nanopositioning system was found experimentally via a broadband FFT-based

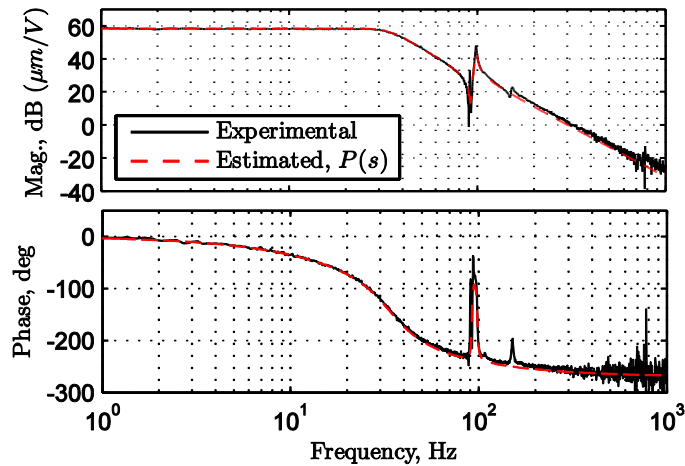


FIGURE 2. OPEN-LOOP FREQUENCY RESPONSE

system identification technique. The Matlab function *invfreqs* was used to fit a fifth-order transfer function, $P(s)$, to the open-loop frequency response. $P(s)$ is given by

$$P(s) = \frac{6.67 \times 10^9}{(s + 157)(s^2 + 156.40s + 4.47 \times 10^4)} \times \frac{(s^2 + 10.22s + 3.34 \times 10^5)}{(s^2 + 14.09s + 3.81 \times 10^5)} \quad (1)$$

Figure 2 shows the experimentally obtained frequency response along with the frequency response of the estimated transfer function from the amplifier command to the measured position. The open-loop bandwidth (-3dB) is approximately 35Hz. The low open-loop bandwidth of the motion system is a consequence of the fundamental limitations in the physical design of MMA and flexure based motion systems [25]. The damping seen in the rigid body mode arises due to eddy currents in the MMA back-iron as well as due to the back-electromotive force dynamics.

LINEAR FEEDBACK DESIGN AND LIMITATIONS

Although the physical system described above is free of friction and backlash, the achievable positioning performance is still limited by various factors as described below:

1. Several sources of noise and disturbance that exist in the system limit the positioning resolution. This includes position sensor noise, actuator driver noise, electronic noise and quantization in the real-time control hardware, and mechanical floor vibrations.
2. The force constant of the MMA is dependent on the moving magnet position with respect to the stator (coils and back-iron). This force-stroke non-uniformity [25] degrades the tracking performance.
3. The non-linearity in the actuator driver also contributes to the tracking error. This nonlinearity shows up as the harmonic distortion at multiples of the fundamental excitation frequency in the command signal. Figure 3 shows one such measurement of the power spectral density of the driver, when the desired output is a 15V, 2Hz sinusoid. The signal-to-noise ratio, which is a measure of the broadband noise, is approximately 120dB. However, the total harmonic distortion, defined as the ratio of power in the harmonics with respect to the power at the fundamental signal frequency, is about -90dB. Since the nonlinearity is less than 0.01%, it is generally very difficult to model it accurately or further reduce it via circuit design.

The estimated open-loop transfer function, $P(s)$ in Eq. (1), is used to design a linear feedback controller $C(s)$ using loop shaping techniques. The controller includes an integrator to ensure zero steady-state error. After considerable iterations and tuning, the following compensator was implemented.

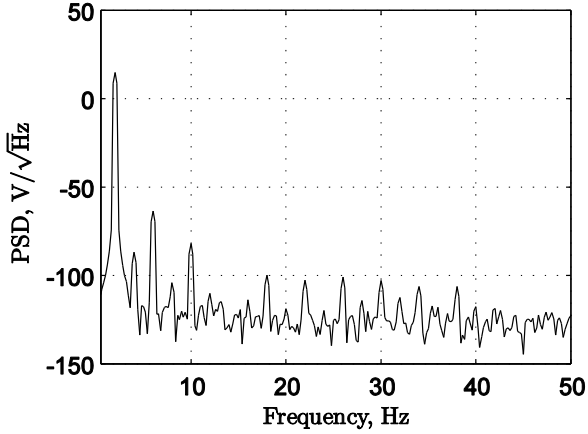


FIGURE 3. HARMONIC DISTORTION IN THE ACTUATOR DRIVER

$$C(s) = \frac{3234(s+147.6)(s^2+156.4s+4.47 \times 10^4)}{s(s+3000)(s^2+4595s+9.05 \times 10^6)} \quad (2)$$

The resulting closed-loop transfer function is given by

$$T(s) = \frac{P(s)C(s)}{1+P(s)C(s)} \quad (3)$$

The frequency response of the closed-loop transfer function in Eq.(3), along with the experimentally obtained closed-loop frequency response, is shown in Figure 4. The phase margin and gain margin for the loop transfer function are 60° and 12dB respectively. The closed-loop bandwidth (-3dB) of the system is approximately 200Hz.

In order to evaluate the tracking performance of the linear feedback controller, a 3mm, 2Hz sinusoidal signal is applied as the command. The resulting tracking error (Figure 5A) is within $\pm 60\mu\text{m}$, which is quite high for nanopositioning. From the power

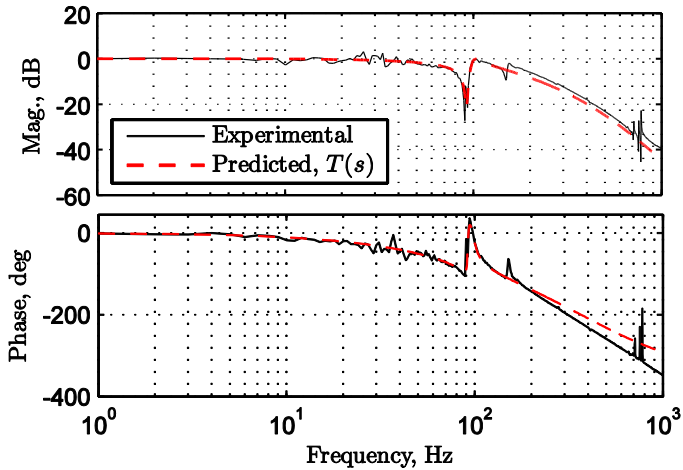


FIGURE 4. CLOSED-LOOP FREQUENCY RESPONSE

spectrum plot of the tracking error, shown in Figure 5C, it is evident that the tracking error consists of broadband noise along with a component at the command signal frequency, as well as the harmonics of the command signal. While the component at 2Hz can be attributed to lack of command following, the higher frequency harmonics are a consequence of the nonlinearities in the actuator and the driver, as mentioned earlier. The feedback controller does provide some reduction in the harmonic content as compared to tracking in an open-loop setting (see Figure 5D). This reduction in the magnitude of the harmonics is a result of sensitivity reduction achieved due to feedback, and can be predicted by plotting the sensitivity transfer function, $S(s)$, which is given by

$$S(s) = \frac{1}{1+P(s)C(s)} \quad (4)$$

Figure 5B shows the Bode magnitude plot of the sensitivity transfer function of the feedback loop. The harmonic component at 10Hz, for example, is suppressed by 20dB, corresponding to the -20dB magnitude of the sensitivity transfer function.

To achieve greater reduction of the harmonics, the sensitivity transfer function, $S(s)$, would have to be reduced further in the low frequency range. However, this can be done only at the cost of decreasing the stability robustness. This is a direct consequence of the analytic design tradeoff associated with the feedback loop, known as the *Bode waterbed effect* [29]. To further explain this, consider the following bounds on the sensitivity and the complementary sensitivity transfer functions:

$$|S(j\omega)| \leq \alpha < 1, \quad \forall \omega \leq \omega_1 \quad (5)$$

$$|T(j\omega)| < \varepsilon \left(\frac{\omega_c}{\omega} \right)^{1+k}, \quad \forall \omega > \omega_c \quad (6)$$

where $\varepsilon < 1/2$ and $k > 0$. Then, it can be shown that [29]

$$\text{Sup}_{\omega \in (\omega_1, \omega_c)} \log |S(j\omega)| \geq \frac{1}{\omega_c - \omega_1} \left\{ \omega_1 \log \left(\frac{1}{\alpha} \right) - \frac{3\varepsilon\omega_c}{2k} \right\} \quad (7)$$

The closed-loop bandwidth constraint in Eq.(6) results from actuator saturation, given the low open-loop plant bandwidth. Also, such constraints are necessary to increase robustness against unmodeled high frequency plant dynamics. Therefore, from Eq.(7), sensitivity reduction at low frequencies can only be achieved by increasing the lower bound of the peak of sensitivity function at intermediate frequencies, which results in loss of stability robustness. This implies that there is a limit to improving the tracking performance of the system by employing a feedback loop because of the low open-loop bandwidth.

From Figure 5C, it can be seen that the deterministic part of the tracking error (due to the nonlinearities as well as due to lack

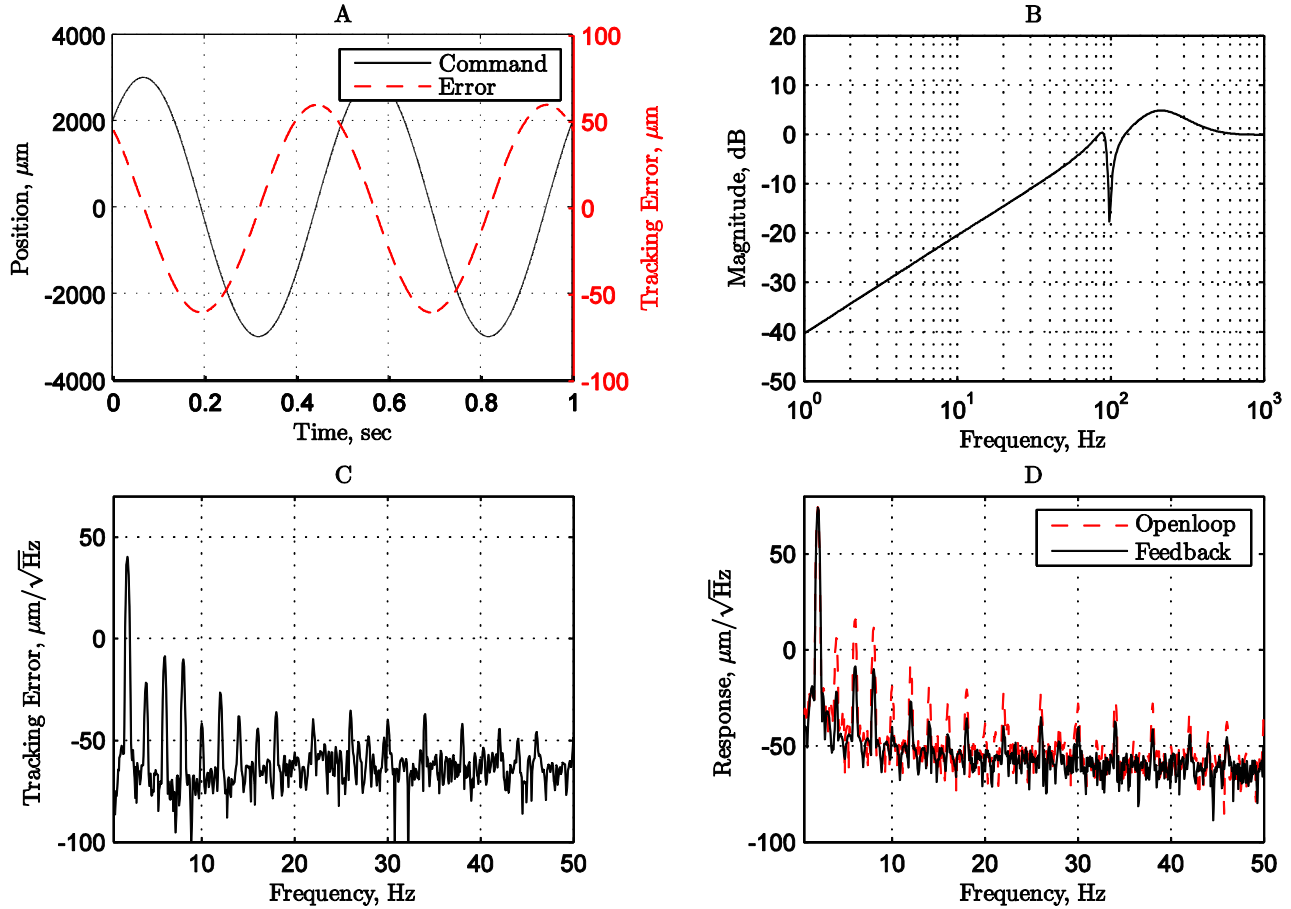


FIGURE 5. TRACKING PERFORMANCE WITH FEEDBACK CONTROL (A). POSITION COMMAND AND TRACKING ERROR (B). SENSITIVITY TRANSFER FUNCTION OF THE FEEDBACK LOOP (C). POWER SPECTRUM OF THE TRACKING ERROR (D). POWER SPECTRUM OF POSITION RESPONSE

of command tracking) is relative large compared to the stochastic part (due to various sources of noise and disturbance mentioned earlier). Moreover, if the command signal is periodic, then the deterministic part of the error also repeats every period. Therefore, in such cases, iterative learning control could be applied in conjunction with feedback in order to reduce the deterministic or the repeating portion of the tracking error [26, 30]. This is done by modifying the control signal based on learning from the error histories obtained during previous iterations.

ITERATIVE LEARNING CONTROL (ILC)

The ILC block diagram incorporated with the feedback loop in shown in Figure 6. Here, P and C denote the plant and the feedback compensator, respectively, of a stable feedback loop. $y_d(t)$ is a periodic command signal and $y(t)$ is the measured response. The objective of ILC is to generate a feedforward command $u(t)$ in order to reduce the tracking error $e(t) = y_d(t) - y(t)$. The tracking error $e_j(t)$ and the ILC input $u_j(t)$ are stored in a memory for every iteration j . The ILC algorithm then evaluates the new input signal, $u_{j+1}(t)$, in an offline manner, to be applied during the next iteration. The iteration period can be chosen as the

command period or any multiple of the command period. This arrangement is also known as the *serial* ILC architecture because the ILC input is added to the command before the feedback loop.

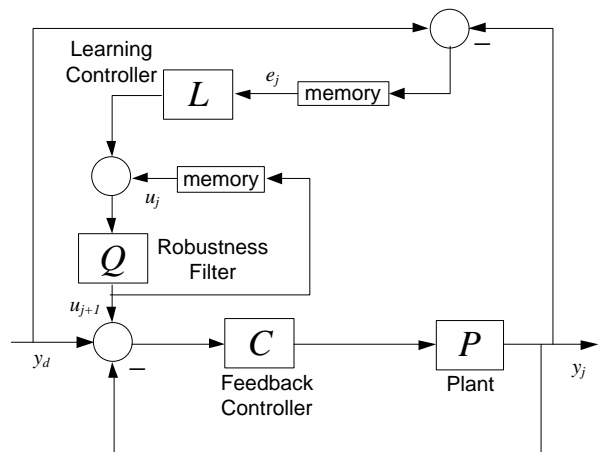


FIGURE 6. ITERATIVE LEARNING CONTROL ARCHITECTURE

A first-order classical ILC update law is given as follows [26]

$$u_{j+1}(t) = Q[u_j(t) + Le_j(t)] \quad (8)$$

where L and Q are called the learning filter and robustness filter, respectively. The design of these filters determines the performance and the robustness of the ILC algorithm as described next [30, 31].

With the assumption that the feedback loop is stable and linear time-invariant, a sufficient condition guaranteeing stability and monotonic convergence of the tracking error in successive iterations is given by the following standard frequency-domain result:

$$|Q(j\omega)[1-L(j\omega)T(j\omega)]| < 1, \quad \forall \omega \quad (9)$$

where $T(s)$ is the closed-loop transfer function of the feedback loop. The error dynamics is given by the following relation

$$(e_\infty - e_{j+1}) = Q(1-LT)(e_\infty - e_j) \quad (10)$$

Additionally, it can be shown that, given the initial tracking error, $e_0(t)$, the tracking error finally converges to

$$e_\infty(t) = \frac{1-Q}{1-Q(1-LT)} e_0(t) \quad (11)$$

From Eq.(10), it can be deduced that the learning filter determines the rate of convergence of error in successive iterations. Specifically, the magnitude of $(1-LT)$ should be small for fast convergence. Since the closed-loop transfer function T is designed to have approximately unity magnitude up to a frequency range of 200Hz (see Figure 4), L is simply chosen as a constant gain $\lambda \leq 1$, resulting in a P-type learning controller. While higher values of λ leads to aggressive learning, smaller gains makes the learning

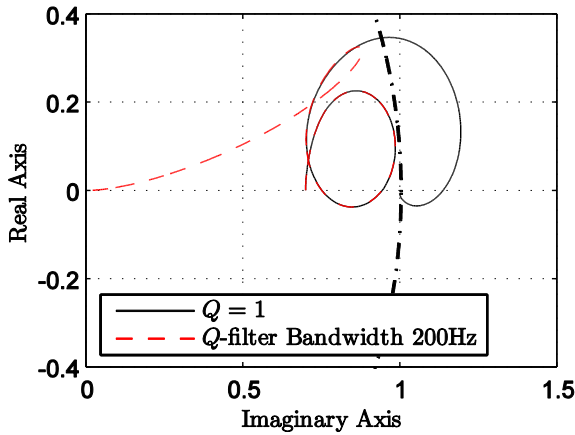


FIGURE 7. NYQUIST PLOT FOR MONOTONIC CONVERGENCE CRITERION

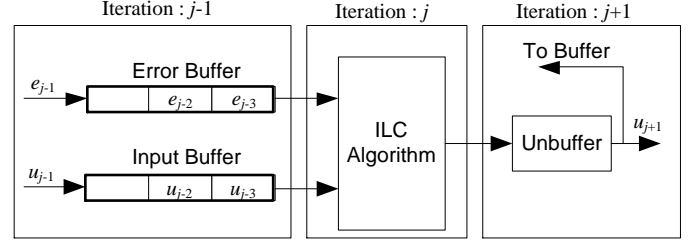


FIGURE 8. ILC OFFLINE IMPLEMENTATION

process less sensitive to noise and leads to lower final errors [26]. Also, because L is a constant gain, it can be easily tuned online while performing experiments.

The robustness filter Q is usually chosen to be a low pass filter with the bandwidth (ω_n) of Q presenting a trade-off between performance and robustness. As seen from Eq.(11), choosing Q as unity ensures convergence to zero tracking error. The Nyquist plot of $Q(1-LT)$ for $\lambda = 0.3$ and $Q = 1$ is shown in Figure 7. The plot goes outside the unit circle at the frequency of about 280Hz, thereby violating the monotonic convergence criterion given in Eq.(9). Hence, the bandwidth of the Q filter is chosen conservatively to be 200Hz. Also plotted in Figure 7 is the Nyquist plot of $Q(1-LT)$ for $\lambda = 0.3$ and $\omega_n = 200$ Hz. The curve remains within unit circle over the entire frequency range. The Q filter is designed as a fifth order Butterworth filter. Moreover, since the filtering is done in an offline manner, Q is designed to be non-causal, using the *filtfilt* function in Matlab, to avoid any phase lag.

Figure 8 shows the scheme adopted for the implementation of the ILC. The error signal $e_{j-1}(t)$ and the ILC input signal $u_{j-1}(t)$ are stored in a memory buffer during the $(j-1)^{\text{th}}$ iteration. The buffers already contain signal values from previous two iterations as shown. During iteration j , these buffers are then used to compute the ILC control for $(j+1)^{\text{th}}$ iteration according to the following modified ILC law:

$$u_{j+1}(t) = Q[u_{j-2}(t) + Le_{j-2}(t)] \quad (12)$$

The resultant ILC control input $u_{j+1}(t)$ is then unbuffered and applied to the feedback loop during the $(j+1)^{\text{th}}$ iteration. The memory buffers contain signal values for 3 iterations in order to facilitate non-causal filtering by taking into account the filter initial conditions. It should be noted that while the feedback computations are done at the sampling rate, the ILC calculation is carried out only once during an iteration.

EXPERIMENTAL RESULTS

The combined feedback and ILC controller described above was applied to the single-axis nanopositioning system. Figure 9 shows the resulting tracking performance for a 3mm, 2Hz sinusoidal command. The learning gain (λ) and robustness filter bandwidth (ω_n) were set to 0.3 and 150Hz, respectively. Figure 9A

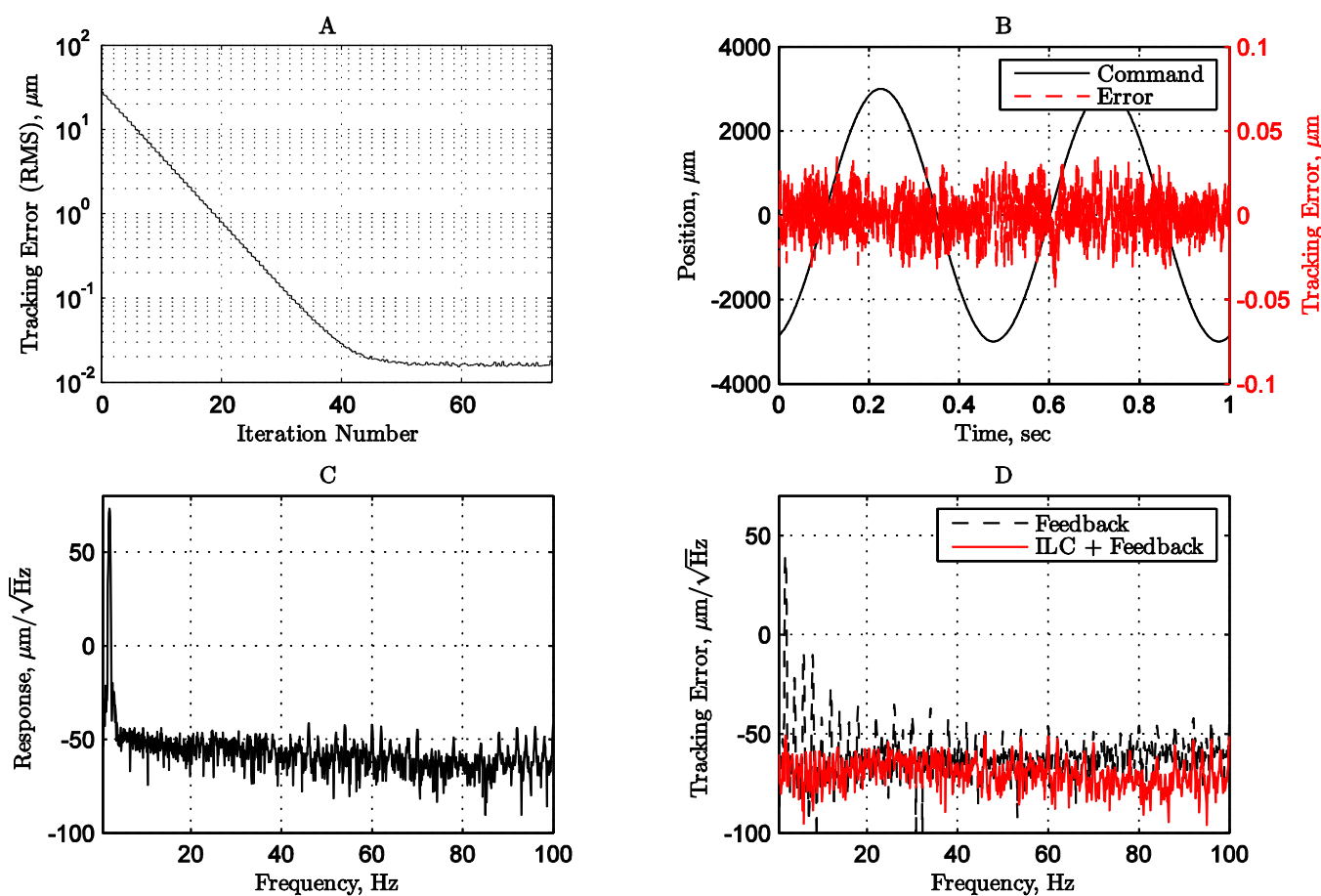


FIGURE 9. TRACKING PERFORMANCE WITH COMBINED FEEDBACK AND ILC (A). TRACKING ERROR CONVERGENCE (B). POSITION COMMAND AND TRACKING ERROR AFTER 60 ITERATIONS (C). POWER SPECTRUM OF POSITION RESPONSE (D). POWER SPECTRUM OF TRACKING ERROR

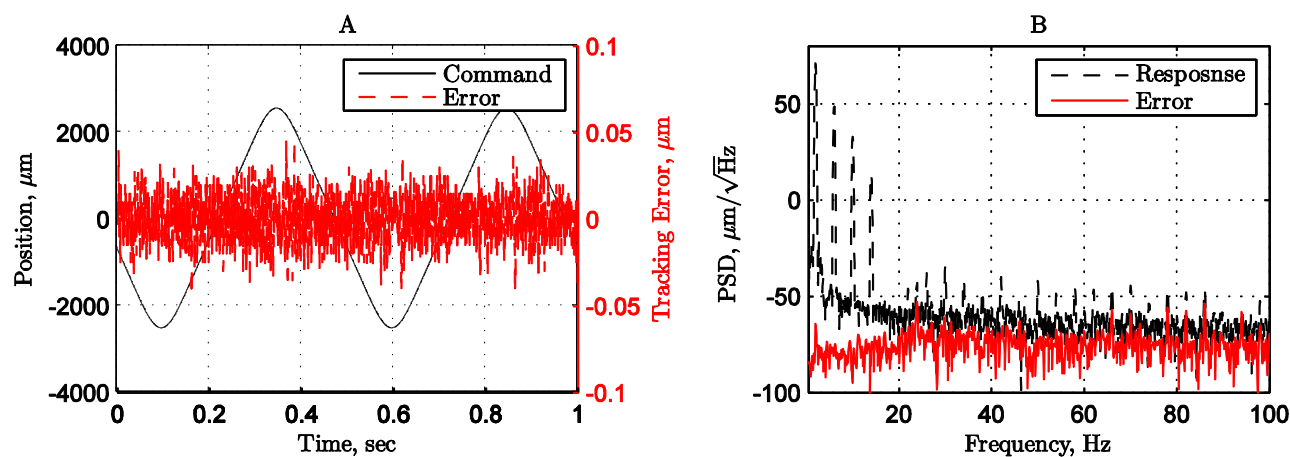


FIGURE 10. TRACKING PERFORMANCE FOR AN OPTIMIZED TRIANGULAR COMMAND (A) TIME RESPONSE (B) POWER SPECTRUM

shows the decrease in the tracking error as a function of the iteration number. The RMS of the tracking error is reduced from 28 μ m to 15nm in approximately 60 iterations. This corresponds to a reduction by a factor of about 1800 in 30 seconds. The tracking error at the end of the 60th iteration is plotted in Figure 9B. The performance improvement, compared to feedback alone, comes from a reduction in the repeating portion of the tracking error at the command frequency and its harmonics (Figure 9D). The power spectrum of the converged position response, shown in Figure 9C, reflects the true dynamic range of the nanopositioning system.

In a separate experiment, a 3mm, 2Hz band-limited triangular waveform was applied as the command. The signal was optimized to have a perfectly linear (constant velocity) region within ± 1.5 mm while minimizing the power content beyond the first three harmonics [32]. The motion speed in the linear region is 24mm/s. As compared to sinusoids, multi-tone command signals are more challenging since they give rise to the intermodulation products in addition to the harmonics. In this case, the tracking error after 60 iterations (Figure 10A) is reduced to 18nm (RMS). The power spectrum of the measured response and the tracking error are shown in Figure 10B.

CONCLUSION

In this paper, an iterative learning controller is applied to improve the tracking performance of a large range single-axis nanopositioning system. In case of periodic commands, the nonlinearities in the moving magnet actuator as well as in the actuator driver produce deterministic and repeating error. While linear feedback alone proves to be inadequate, a P-type serial-architecture learning controller in conjunction with this linear feedback is shown to reduce the tracking error by more than three orders of magnitude. However, the tracking error is still 4 to 5 times larger than the sensor resolution. In future, other choices of learning filter [30] will be investigated to further improve the tracking performance as well as to improve the rate of convergence.

ACKNOWLEDGMENTS

This work was supported in part by a National Science Foundation Grant (CMMI # 1100807). The first author acknowledges a Measurement Science and Engineering Fellowship from the National Institute of Science and Technology.

REFERENCES

[1] Devasia, S., et al., 2007, "A Survey of Control Issues in Nanopositioning," *Control Systems Technology, IEEE Transactions on*, 15(5), pp. 802-823.
[2] Awtar, S., and Parmar, G., 2010, "Design of a large range XY nanopositioning system," *ASME International Design Engineering Technical Conferences and Computers and Information in Engineering Conference, IDETC/CIE2010*, pp. 387-399.

[3] O'Brien, W., 2005, "Long-range motion with nanometer precision," *Photonics Spectra*, 39(6), pp. 80-81.
[4] Sinno, A., et al., 2007, "Enlarged atomic force microscopy scanning scope: Novel sample-holder device with millimeter range," *Review of Scientific Instruments*, 78(9), pp. 095107-095107.
[5] Salaita, K., et al., 2007, "Applications of dip-pen nanolithography," *Nat Nano*, 2(3), pp. 145-155.
[6] John, A. K., 2005, "Nanometre resolution metrology with the Molecular Measuring Machine," *Measurement Science and Technology*, 16(11), p. 2121.
[7] Maeda, G. J., and Sato, K., 2008, "Practical control method for ultra-precision positioning using a ballscrew mechanism," *Precision Engineering*, 32(4), pp. 309-318.
[8] Chassigne, L., et al., 2007, "A 2D nano-positioning system with sub-nanometric repeatability over the millimetre displacement range," *Measurement Science and Technology*, 18(11), pp. 3267-3272.
[9] Lihua, L., et al., 2010, "Design and Testing of a Nanometer Positioning System," *Journal of Dynamic Systems, Measurement, and Control*, 132(2), pp. 021011-021016.
[10] Buice, E. S., et al., 2009, "Design evaluation of a single-axis precision controlled positioning stage," *Precision Engineering*, 33(4), pp. 418-424.
[11] Young-Man, C., et al., 2008, "Design and control of a nanoprecision XY scanner," *Review of Scientific Instruments*, 79(4), pp. 045109-045101.
[12] Zschaecck, S., et al., 2011, "Decentralized high precision motion control for nanopositioning and nanomeasuring machines," *IECON 2011 - 37th Annual Conference on IEEE Industrial Electronics Society*, pp. 546-551.
[13] Michellod, Y., et al., 2006, "Strategy for the Control of a Dual-stage Nano-positioning System with a Single Metrology," *Robotics, Automation and Mechatronics, 2006 IEEE Conference on*, pp. 1-8.
[14] Kosinskiy, M., et al., 2006, "Tribology of nanopositioning characterization of precision linear bearings on nanometre scale," *VDI Berichte(1950)*, pp. 215-224.
[15] Holmes, M., et al., 2000, "Long-range scanning stage: A novel platform for scanned-probe microscopy," *Precision Engineering*, 24(3), pp. 191-209.
[16] Kim, W.-J., and Verma, S., 2007, "Multiaxis maglev positioner with nanometer resolution over extended travel range," *Journal of Dynamic Systems, Measurement and Control, Transactions of the ASME*, 129(6), pp. 777-785.
[17] Khan, M. U., et al., 2011, "A Long Stroke Electromagnetic XY Positioning Stage for Micro Applications," *Mechatronics, IEEE/ASME Transactions on*, PP(99), pp. 1-10.
[18] Dejima, S., et al., 2005, "Dynamic modeling, controller design and experimental validation of a planar motion stage for precision positioning," *Precision Engineering*, 29(3), pp. 263-271.
[19] Shinno, H., et al., 2004, "X-Y- θ Nano-Positioning Table System for a Mother Machine," *CIRP Annals - Manufacturing Technology*, 53(1), pp. 337-340.

- [20] Maeda, G. J., et al., 2006, "Control of an XY nano-positioning table for a compact nano-machine tool," *JSME International Journal, Series C (Mechanical Systems, Machine Elements and Manufacturing)*, 49(1), pp. 21-27.
- [21] Kang, D., et al., 2009, "Optimal design of high precision XY-scanner with nanometer-level resolution and millimeter-level working range," *Mechatronics*, 19(4), pp. 562-570.
- [22] Fukada, S., and Nishimura, K., 2007, "Nanometric positioning over a one-millimeter stroke using a flexure guide and electromagnetic linear motor," *International Journal of Precision Engineering and Manufacturing*, 8(2), pp. 49-53.
- [23] Aoyama, T., et al., 2009, "Numerical and experimental analysis of transient state micro-bounce of aerostatic guideways caused by small pores," *CIRP Annals - Manufacturing Technology*, 58(1), pp. 367-370.
- [24] Chen, X., et al., 2011, "Air vortices and nano-vibration of aerostatic bearings," *Tribology Letters*, 42(2), pp. 179-183.
- [25] Parmar, G., et al., 2011, "Design, Fabrication, and Testing of a Moving Magnet Actuator for Large Range Nanopositioning," *ASME Dynamic Systems and Control Conference*.
- [26] Longman, R. W., 2000, "Iterative learning control and repetitive control for engineering practice," *International Journal of Control*, 73(10), pp. 930-954.
- [27] Otten, G., et al., 1997, "Linear motor motion control using a learning feedforward controller," *IEEE/ASME Transactions on Mechatronics*, 2(3), pp. 179-187.
- [28] Steinbuch, M., and Molengraft, M. J. G. V. D., 2000, "Iterative learning control of industrial motion systems," *Proc. 1st IFAC Conference on Mechatronic Systems*, pp. 967-972.
- [29] Freudenberg, J. S., Looze, D. P., 1988, *Frequency Domain Properties of Scalar and Multivariable Feedback Systems*, Springer-Verlag, Berlin
- [30] Bristow, D. A., et al., 2006, "A survey of iterative learning control," *Control Systems, IEEE*, 26(3), pp. 96-114.
- [31] Norrlöf, M., and Gunnarsson, S., 2002, "Time and frequency domain convergence properties in iterative learning control," *International Journal of Control*, 75(14), pp. 1114-1126.
- [32] Fleming, A. J., and Wills, A. G., 2009, "Optimal periodic trajectories for band-limited systems," *IEEE Transactions on Control Systems Technology*, 17(3), pp. 552-562.